HHS Public Access

Author manuscript

*Curr Protoc Cytom*. Author manuscript; available in PMC 2019 July 01.

Published in final edited form as:

*Curr Protoc Cytom*. 2018 July ; 85(1): e41. doi:10.1002/cpcy.41.

# Mitochondrial Subtype Identification and Characterization

**Joseph R. Daniele**[*,1], **Kartoosh Heydari**[2], and **Andrew Dillin**[*,1]

[1]Department of Molecular & Cellular Biology, University of California, Berkeley, Berkeley, CA 94720

[2]LKS Flow Cytometry Core, Cancer Research Laboratory, University of California, Berkeley, Berkeley, CA 94720

## Abstract

Healthy, functional mitochondria are central to the maintenance of many cellular and physiological phenomena, including aging, metabolism, and stress resistance. A key feature of healthy mitochondria is a high membrane potential ($\Delta\psi$) or charge differential between the matrix and inner mitochondrial membrane. Mitochondrial $\Delta\psi$ has been extensively characterized via flow cytometry in the context of intact cells, in which an average signal is generated across all the mitochondria contained within a cell. However, mitochondrial populations differ dramatically even within a single cell, and thus interrogation of mitochondrial quality at the organelle level is necessary to better understand and accurately measure this heterogeneity. Here we describe a new flow cytometric methodology that enables the quantification and classification of mitochondrial subtypes (via their $\Delta\psi$, size, and substructure) using the small animal model *C. elegans*. Future application of this methodology should allow research to discern the bioenergetic and mitochondrial component in a number of human disease and aging models (e.g. *C. elegans*, cultured cells, small animal models, and human biopsy samples).

### Keywords

isolated organelle; mitochondrial subtypes; flow cytometry; individual organelle analysis; tissue-specific organelle analysis

## Introduction

### Mitochondrial Subtype Identification and Characterization via Flow Cytometry

Organismal bioenergetics is at the heart of a wide array of cellular and physiological phenomena. Although tissue-specific mitochondrial dysfunction (e.g. brain, muscle, liver) has been described for multiple mitochondrial diseases, methods to characterize mitochondrial heterogeneity and tissue-specific variation in mitochondrial function have been lacking (Sharpley et al., 2012; Ylikallio and Suomalainen, 2011). One method of measuring mitochondrial health is their membrane potential ($\Delta\psi$), or charge differential

*Co-corresponding Authors: jdaniele@berkeley.edu & dillin@berkeley.edu.

**Conflicts of Interest**

None to report.

between the matrix and inner mitochondrial membrane, a feature of strong electron transport chain-mediated ATP generation. Using the ratiometric dye, JC-1, flow cytometry has been applied to the study of mitochondrial $\Delta\psi$ in single cells and isolated mitochondria (Parone et al., 2008; Cossarizza and Salvioli, 2001; Gravance et al., 2000; Chen et al., 2005; Adhihetty et al., 2005; Smiley et al., 1991; Saunders et al., 2013; Cossarizza et al., 1996; Vander Heiden et al., 1997; Narendra et al., 2008). JC-9, the dye used in this study, is a similarly small, ratiometric, cyanine dye, but is more lipophilic than JC-1. It accumulates in the mitochondrial matrix as both a green "monomeric" and a red "aggregate" fluorescent form. Upon being driven into the interior-negative mitochondrial matrix, its monomer can accumulate there independent of membrane potential. Formation of the red aggregate state, conversely, increases as mitochondria become more polarized (Figure 4A). JC-9 was chosen over comparable mitochondrial dyes because of its high signal to noise ratio in labeling mitochondria (>10-fold above controls), ratiometric properties (which enable size-normalized $\Delta\psi$ measurement) and compatibility with blue-fluorescent proteins (for tissue-specific mitochondrial studies). Utilizing JC-9, in conjunction with flow cytometry, enables highly sensitive measurements of organelle features (e.g. $\Delta\psi$, size, and substructure) for any tissue across animals of any age, and is an effective complement to microscopy-based studies of mitochondria. Notably, while our data suggests that isolated mitochondria respire normally and resemble the size, substructure, and $\Delta\psi$ measured *in vivo* we cannot rule out the possibility that our method might cause some sampling bias due to disruption of the *in vivo* mitochondrial network prior to tissue homogenization (see Daniele et al., 2016 for a discussion of quantitative comparisons against conventional isolation techniques for mitochondrial mass yield and *in vivo* vs. *in vitro* mitochondrial properties). Nonetheless, the ability to define multiple energetic subtypes (similar to previously described reports) indicates our method is applicable and practical in this space.

## *BASIC PROTOCOL 1.* MITOCHONDRIAL SUBTYPE IDENTIFICATION AND CHARACTERIZATION IN *C. ELEGANS* VIA FLOW CYTOMETRIC ANALYSIS

While the identification and characterization of mitochondrial subtypes is paramount to understanding the pathology and tissue etiology of mitochondrial disease, the ability to isolate and characterize mitochondrial membrane potential ($\Delta\psi$) from the nematode, *Caenorhabditis elegans (C. elegans*), has not been demonstrated. Since $\Delta\psi$ perturbation has been associated with lifespan extension, fertility, apoptosis, and increased heat resistance in nematodes, we applied flow cytometry to analyze $\Delta\psi$ in isolated mitochondria (Brys et al., 2010; Kuang and Ebert, 2012; Lemire et al., 2009; Tsang and Lemire, 2002; Jagasia et al., 2005; Hicks et al., 2012). Notably, the small size, fast generation time, transparent cuticle, and multicellularity (nervous system, digestive system, musculature) of this organism has made it well-suited to aging and mitochondria research. To date, most *C. elegans* research in mitochondria has been done via microscopy. Studies using isolated mitochondria are rare due to the difficulty in isolating high quality mitochondria from nematodes, particularly due to their tough outer cuticle. Flow cytometry has been previously used to to analyze reactive oxygen species in isolated *C. elegans* mitochondria (Yang and Hekimi, 2010). Here we describe a new flow cytometry approach to [1] isolate *C. elegans* mitochondria and analyze

$\Delta\psi$ and [2] demonstrate the potential of this approach to identify mitochondrial subtypes based on their bioenergetics and morphology.

## Materials

~2,000–10,000 wild-type (e.g. N2) *C. elegans* nematodes (or eggs), per sample or isolate, synchronized at optimal growth temperature (e.g. 20° C) using previously published developmental timing and worm growth media (Brenner, 1974; Byerly et al., 1976).

1 mM JC-9 (3,3′-Dimethyl-α-naphthoxacarbocyanine iodide) (D-22421, Thermo Fisher) in DMSO

10 mM valinomycin (V0627, Sigma Aldrich) in DMSO

Collagenase Type 3 (“Collagenase 3 enzyme”, CLS 3- LS004182, Worthington)

Protease Inhibitor Cocktail (539134, Calbiochem)

Glass Pasteur pipettes (9 inch, VWR)

Glass homogenizer (2 mL with small clearance pestle (0.07 mm), Kimble chase)

0.22 μm Tube Top Filters (50 mL polystyrene, 430320, Corning)

0.22 μm-filter-sterilized Collagenase 3 buffer (See reagents and solutions)

Autoclaved M9 Buffer (See reagents and solutions)

0.22 μm-filter sterilized Mitochondria Isolation Buffer (MIB) + Protease Inhibitor Cocktail (1:1000) (See reagents and solutions)

15 mL centrifuge tubes with screw caps (21008-216, VWR)

1.7 mL microcentrifuge tubes (MCT-175-C-S, Axygen)

5 mL polystyrene round-bottom tubes (352052, Falcon)

Table-top centrifuge that accommodates 15 mL conical tubes (e.g. Eppendorf Centrifuge 5702R with a 5702/R A-4-38 rotor and IL025 swinging buckets with plastic inserts)

Table-top refrigerated centrifuge set to 4° C (e.g. Eppendorf Centrifuge 5424R with the 5424/R rotor with screw-on lid, FA-45-24-11).

BD LSR Fortessa Analyzer with the following filters: forward scatter (FSC), side scatter (SSC, “Granularity/Substructure”) (488 nm/10), FITC (“Green channel”) (525 nm/50 with a 500 nm Long Pass filter), and PE-Tx-Red YG (“Red channel”) (610 nm/20 with a 600nm Long Pass filter).

FACS Rinse (340346, BD Bioscience) or 5% Contrad 70 Solution (Decon. Labs, 1002)

Duke Standards (NIST Traceable Polymer Microspheres, catalog #3K-200, 3K-400, 3K-700, and 3K-1000, ThermoFisher)

FlowJo v10 software (or a comparable software program)

## Part I: Mitochondrial Isolation from C. elegans (adapted from Gandre and van der Bliek, 2007)

1 Wash worms off plates using 14 mL of M9 and transfer to a 15 mL tube. Spin down for 30 seconds at 1000xG in a table top centrifuge at room temperature. Aspirate M9 (leaving worm pellet unperturbed).

***Mitochondrial isolation from cultured cells is detailed in** Nguyen et al., 2017. ***Since cultured cells do not have to be homogenized into individual cells, we lysed cell pellets using 5 passes through a 27½ gauge needle. All downstream steps were identical. We have confirmed this isolation technique works with mouse cells (e.g. mouse embryonic fibroblasts (MEFs),** Nguyen et al., 2017) ***and various human cell lines. Additional materials needed for this isolation will include a Luer-Lok Tip syringe (5 mL, BD) and needle (27.5G, BD).***

2 Resuspend worms in 10 mL of filter-sterilized Collagenase 3 buffer with Collagenase 3 enzyme [final 1 mg/mL] added and gently agitate for 1 hour at 20° C (Cox et al., 1981).

3 Dilute out collagenase from worm mix on ice with 3 serial washes of autoclaved M9 buffer. In between the washes, spin down worms at room temperature, and aspirate M9 down to the pellet as in Step 1.

4 Add 500 μL of chilled MIB buffer to worm pellet, transfer to a glass homogenizer (via a 9-inch glass Pasteur pipette), and homogenize with ~18 strokes.

***A simple method to determine if the worms are sufficiently homogenized is to look at a sample of the lysate and check under a dissecting microscope if worm carcasses are broken up and visibly split open.***

5 Transfer lysate to 1.7 mL microcentrifuge tubes using a glass Pasteur pipette and add 0.5 μL of JC-9 stock solution [final 10 μM].

***Include two to three extra tubes in the spins to use for proper flow cytometry controls. These include [1] a tube that consists only of MIB and JC-9 dye to identify pelleted dye aggregates and [2] a tube that consists only of lysate (no dye added) so that unlabeled mitochondria can be identified and [3] if using mitochondria that can be identified in any other way, e.g. with a blue fluorescent protein (see** Daniele et al., 2016, Figure 4), ***include a "no dye" control of this lysate as well.***

***A minimum of three technical replicates are recommended for every biological replicate performed.***

6 Spin tubes at 200xG for 5 minutes at 4° C in a table-top centrifuge (see Figure 1).

Tubes are to stay on ice when not in the centrifuge.

7 Carefully remove ~400 μL of the supernatant (leave ~100 μL so as not to disturb the pellet), transfer to fresh microcentrifuge tubes, and spin at 800xG for 10 minutes at 4° C.

Pellet in the first two spins should consist of nuclei, whole cells, worm carcasses, and unbound dye aggregate.

8 Transfer ~300 μL of the supernatant to fresh tubes, again leaving ~100 μL and spin the supernatant at 12,000xG for 10 minutes at 4° C.

Pellet in the third, and final, spin should include **mitochondria**, lysosomes, and peroxisomes.

9 Remove ~200 μL of supernatant, leaving ~100 μL. Resuspend these mitochondria (which are enriched in the pellet and should maintain their *in vivo* membrane potential, "polarized," for up to 3 hours on ice) in 500 μL chilled, filtered MIB. Analyze samples on flow cytometer, ideally, within 1 hour of isolation.

***If samples are kept on ice, a membrane potential will persist for up to 3 hours after mitochondrial isolation. However, a noticeable drop in the magnitude and range of the JC-9 ratio has been observed following 1 hour on ice.***

## Part II: Running Samples on the Flow Cytometer

10 Transfer isolated mitochondria to 5 mL round-bottom tubes on ice.

11 To avoid background noise from the flow cytometer fluidic system, run 10% bleach for 5 minutes, then FACS Rinse (or 5% Contrad) for 5 minutes, followed by 0.1 μm filtered DI-water for 15 minutes.

When running the samples, use a low flow rate (e.g. <1000 particles/minute) while collecting the data. This is important when using a Fortessa with a hydrodynamic focusing system. In our experience, we have observed minimal differences in data quality and consistency with a flow rate of 10,000 particles/minute but still recommend starting at a lower flow rate and then moving up.

12 To avoid mitochondrial aggregates from analysis, use combinations of pulse-Area (FSC-A, SSC-A), pulse-Height (FSC-H, SSC-H), and pulse-Width (FSC-W, SSC-W) as follows: [1] FSC-A vs. FSC-H, [2] SSC-H vs. SSC-W, [3] FSC-H vs. FSC-W. This will progressively gate clusters/populations that increase linearly and help identify the singlet population for further analysis.

13 Identify labeled mitochondria from the crude lysate by standard, sequential gating of linearly-variable clusters: [1] pulse channels (FITC-A vs. FSC-A) and if using blue-fluorescently labeled mitochondria, also [2] pulse channels (FITC-A vs. PacBlue-A) (see Figure 2). We suggest using biexponential scaling to visualize fluorescence in the FITC and PE channels for singlet mitochondria

during data acquisition. This scale enables one to simultaneously observe values between 0 and 10 on a linear scale and values above 10 on a logarithmic scale.

For JC-9, recorded channels should be: forward scatter (FSC, "Size"), side scatter (SSC, "Granularity") (488 nm/10), FITC ("Green channel") (525 nm/50 with a 500 nm Long Pass filter), and PE-Tx-Red YG ("Red channel") (610 nm/20 with a 600nm Long Pass filter). To reduce spectral overlap we applied an 8.5% compensation between the PE and FITC channels and a 1% compensation between the FITC and PE channels.

*If you are interested in also identifying blue-fluorescently labeled mitochondria (e.g. for tissue specific studies, as in Figure 4 of* Daniele et al., 2016), *one should include Pacific Blue ("Blue channel") (450 nm/50) in the recorded channels. One should also run a sample that contains unlabeled, blue-fluorescent mitochondria (see* Figure 2).

Although all data points should be recorded, calibrate laser power and acquisition settings (channel compensation) to nullify any signal from dye aggregates or unlabeled mitochondria (see Part I, Step 5). Further, gating for singlets should be performed to calibrate channels to levels of "single mitochondria" fluorescence.

**14** Determine the gating of each fluorescent channel by comparing a control sample without any fluorescent labeling (tubes [1] & [2] from *Part I, Step 5*) and a control that was labeled in a single channel (e.g. tube [3] from *Part I, Step 5*).

Collect at least 100,000 singlet events on flow cytometer for each sample.

*Use size calibration beads to extrapolate mitochondrial diameter (see* Figure 3). |

**15** Once all "polarized" mitochondria samples are run (i.e. at least 100,000 particles recorded per sample, see Figure 2), transfer 250 μL of each sample to a new tube and add 0.3 μL of valinomycin [final 12 μM] to "depolarize" the sample.

Be sure to also add valinomycin to the "lysate alone" and "dye alone" controls to enable gating out of valinomycin aggregates.

Keep thawed valinomycin at room temperature. Even a small amount (~50 μL) will take at least 10 minutes to thaw once it has been on ice.

*To allow for depolarization, $K^+$ was included in the MIB. Previous reports have shown that isolated mitochondria can polarize and respire normally as long as a "permeant ion" such as $K^+$ is present in the buffer, particularly in the absence of an ETC substrate (e.g. succinate)* (Gómez-Puyou et al., 1970; Ogata and Rasmussen, 1966; Knight et al., 1981). *Moreover, since valinomycin is a $K^+$ ionophore, it requires this ion to depolarize mitochondria. Valinomycin has been used in*

*conjunction with JC dyes in several other studies* (Reers et al., 1991; Cossarizza et al., 1993; Wolken and Arriaga, 2014).

Depolarization is important to establish the "ground state" $\Delta\psi$ of the isolated mitochondria. This will be an important value when deciding where different subdivisions of mitochondrial subtypes lie.

**16** Let tubes with "depolarized" mitochondria sit on ice for 3–5 minutes before running again on the flow cytometer.

**17** When all samples have been run, save and export as .FCS files.

## Part III: Statistical Analysis of Flow Cytometric Data for Mitochondrial Subtype Identification

**18** Open all .FCS files into a FlowJo v10 workspace (or use a comparable software program).

**19** For the "unlabeled mitochondria" sample, define gating for "singlets" (or single mitochondria) using the sequential gates of *Part II, Step 12*.

*Mitochondrial diameter is determined by extrapolating from forward scatter (FSC) data acquired using standardized polymer microspheres (beads). Calculations should be based on flow cytometric readings from that experiment. For example, mitochondria diameter (nm) = y = 123.08*(FSC)^0.244,* $R^2$ *= 0.998, Residual sum of squares (RSS) = 467.31 (see* Figure 3). *This method to approximate mitochondrial size has been previously reported* (Beavis et al., 1985; Knight et al., 1981; Petit, 1992).

**20** Identify "dye-labeled" mitochondria by sequentially modifying the gate to exclude: [1] unlabeled mitochondria, [2] aggregated dye, and [3] aggregated valinomycin and aggregated JC-9 dye (e.g. *Part II, Step 15*) from any exported data (e.g. using *FITC-A* vs. *FSC-A*)

*If tissue-specific studies that require identifying blue-fluorescently labeled mitochondria (e.g. from a particular nematode tissue like the muscle, e.g.*Figure 4 *from* Daniele et al., 2016) *are being performed, gating should include the blue channel (e.g. FITC-A vs. PacBlue-A). For the experiments using blue-labeled ("BFP positive") mitochondria, only blue fluorescent mitochondria that had blue signal and green signal (to indicate JC-9 labeling) above background should be counted as BFP positive mitochondria.*

**21** When defined mitochondrial populations have been established, export the gated populations as .CSV files and open in Microsoft Excel (preferably with the Sigma XL add-on) to perform statistical analyses. The recommended channels to export are: *FSC-A*, *SSC-A*, *FITC-A*, *TxRed-A*, "Membrane Potential" (*TxRed-A*/*FITC-A* for each particle), and "Mitochondrial Diameter" (computed from *FSC-A*).

*A "function" was created in the FlowJo workspace to automatically compute "Mitochondrial Diameter" (using the equation from Part III, Step 19) and "Membrane Potential" (using the ratio of Red to Green JC-9 signal) (see* Figure 4).

*The ground state of $\Delta\psi$ was established by setting a division point above the max Red/Green JC-9 ratio for all the "depolarized" samples (see* Figure 5 *and also* Figures 3C *and S3 in* Daniele et al., 2016).

The data in these experiments did not possess a Gaussian distribution (by Anderson Darling test) and thus we performed only non-parametric tests for significance (e.g. Mann-Whitney). We recommend testing the normality of your data before deciding on whether to perform a parametric or non-parametric test.

## REGENTS AND SOLUTIONS

0.22 μm-filter sterilized Collagenase 3 buffer [100 mM Tris-HCl, pH 7.4, 1 mM $CaCl_2$]

*Adapted from* Cox et al., 1981 - *For 250 mL of buffer: (1) add 0.037 g of $CaCl_2$ dihydrate to 25 mL of 1 M Tris HCl (pH 7.4), (2) add distilled milliQ $H_2O$ to 200 mL and mix using a stir bar, (3) pH the solution to 7.4, (4) add to 250 mL with distilled milliQ $H_2O$, (5) filter sterilize using a 0.22 μm filter (e.g. #430767 from Corning). Stable for 6 months at room temperature.*

M9 Buffer [42 mM $Na_2HPO_4$, 22 mM $KH_2PO_4$, 86 mM NaCl, and 1mM $MgSO_4.7H_2O$]

For 1 L of buffer: (1) Dissolve 3 g $KH_2PO_4$ (monobasic), 6 g $Na_2HPO_4$, and 5 g NaCl in up to 1 L of $H_2O$ with a stir bar, (2) Aliquot into multiple volumes (e.g. 500 mL), (3) Autoclave 25–30 minutes, (4) using sterile technique, allow media to cool to 55–60° C, (5) add 2 mL of 0.5 M $MgSO_4$ per 1 L of solution (or 200 uL per 100 mL solution). Stable at room temperature indefinitely if unopened or 3 months once opened.

0.22 μm-filter sterilized Mitochondria Isolation Buffer (MIB) [50 mM KCl, 110 mM Mannitol, 70 mM Sucrose, 0.1 mM EDTA (pH 8.0), 5 mM Tris-HCl (pH 7.4), with Protease Inhibitor Cocktail (1:1000 dilution) added fresh]

For 250 mL of buffer: (1)mix 2.5 mL of 2.5 M KCl, 55 mL of 0.5 M Mannitol, 17.5 mL of 1 M Sucrose, 50 mL of 0.5 M EDTA (pH 8.0), and 1.25 mL of 1 M Tris-HCl (pH 7.4) using a stir bar, (2) add distilled milliQ $H_2O$ to 200 mL, (3) pH the solution to 7.4, (4) add to 250 mL with more distilled milliQ $H_2O$, (5) filter sterilize using a 0.22 μm filter (e.g. #430767 from Corning). Stable for 6 months at 4° C.

Before mitochondrial isolation, add 1 μL of Protease Inhibitor Cocktail for every 1000 μL of MIB you plan to use, mix by vortexing, filter sterilize using a 0.22 μm filter (e.g. #430320 from Corning), and keep on ice.

# COMMENTARY

## Background Information

The use of highly sensitive flow cytometry enabled the distinction of mitochondrial properties ($\Delta\psi$, size, substructure/granularity) at the individual organelle level, which provides a basis for identification, classification, and characterization of mitochondrial subtypes in *C. elegans*. The method could be widely applicable to mitochondria isolated from any stage in the nematode lifespan (e.g. developing or aged animals), any tissue (e.g. muscle, intestine, neurons), or a combination of both applications (e.g. mitochondria from aged tissues). While we focused on JC-9 as an indicator of $\Delta\psi$, our protocols could be modified to use with other reporter dyes (e.g. MitoSOX to measure reactive oxygen species, Yang and Hekimi, 2010, or tissue-specific BFP-labeled mitochondria and Mitotracker Red-labeled mitochondria, Daniele et al., 2016). Recently, a variant of our method was used to characterize mitochondrial heteroplasmy across *C. elegans* tissues (Ahier et al., 2018). We have also applied this technique to measure the effect certain lipids exert on the properties of isolated mitochondria (Nguyen et al., 2017). Finally, although we applied this approach to *C. elegans* because of its prevalence as a model for development, disease pathology, toxicity, and aging, it is envisioned that this could also be applied to monitor the $\Delta\psi$ of mitochondria isolated from cell culture, other model organisms, or tissue biopsies. This new tool should enable in-depth study of mitochondrial bioenergetics, which is critical in multiple fields of biomedical research.

## Critical Parameters

This protocol was designed to enable a fast, quantitative analysis of mitochondrial $\Delta\psi$ and morphology from a small amount of crude isolate. The purity and yield of mitochondria in our protocol appears to preserve the yield of mitochondrial mass, maintain mitochondrial integrity, and not effect mitochondrial respiration (Daniele et al., 2016). We have also demonstrated that functional measurements performed on “mitochondrial particles” (*in vitro*) are highly associated with their *in vivo* counterparts (Daniele et al., 2016) but we acknowledge that these measurements cannot be quantitatively compared (Degli Esposti, 2001; Cottet-Rousselle et al., 2011).

Our choice of homogenizer was made with several considerations in mind. First, worms are much less likely to stick to glass than to other surfaces (e.g. metal). Second, while we are aware that glass homogenizers tend to be more variable in their clearance than metal homogenizers this “gentler” homogenization method was found to yield similar mitochondrial mass but led to increased mitochondrial integrity (Daniele et al., 2016). Perhaps these reasons are why glass homogenizers are considered the “gold standard” for *C. elegans* organelle isolation. Finally, all points in this protocol were optimized to decrease the variability of inter-sample variation (e.g. buffer composition and depolarizing the same sample) and to maximize the number of samples that can be run reliably (e.g. 30 *C. elegans* samples per day). Depending on experimental conditions required, an additional mitochondrial purification step (e.g. using density gradient centrifugation) may be necessary. For example, the protocol described here was successfully used to observe the effects of

lipids on $\Delta\psi$ in isolated mitochondria (Nguyen et al., 2017) but other metabolites, chemicals, or lipids may not be compatible with our rapid isolation protocol.

## Troubleshooting

If you are using this technique for the first time, we recommend starting with a tissue or protocol where you expect mitochondria to have a high membrane potential (e.g. at least 1.3x higher JC-9 ratio for polarized:depolarized). We have had success with differentiation paradigms (e.g. larval stages in *C. elegans*, differentiation of cultured cells) and with high ATP demanding tissues (e.g. muscle). In our hands, the dynamic range of JC-9 ratios has been smaller in immortalized cell culture and thus, more difficult to measure differences between “polarized” and “depolarized”. If this is the case, we recommend adding agents that will facilitate mitochondrial respiration (e.g. succinate, see buffers used in Wolken and Arriaga, 2014).

While mitochondria in their cellular environment may adopt a variety of shapes and conformations, once they are isolated, mitochondria become spherical (Claude and Fullam, 1945; Yamada et al., 2009; Shimada et al., 1978; O’Toole et al., 2010). Therefore we assume that microspheres can be used appropriately for approximating mitochondrial diameter. One noteworthy example, which demonstrates the fidelity of our mitochondria size estimates comes from the near identical diameter values we found for nematode muscle mitochondrial between flow cytometry and *in vivo* confocal micrographs (Daniele et al., 2016; Head et al., 2011).

If mitochondria are unusually stressed in the experimental setup, several considerations should also be kept in mind. It has been reported that autofluorescence (esp. with emission between 450 and 550 nm) has been observed to vary from “stressed” mitochondria (e.g. oxidative stress, radiation stress, protein aggregation) compared to unstressed controls (Bartolomé and Abramov, 2015; Andersson et al., 1998; Monici, 2005; Bondza-Kibangou et al., 2001; Schaue et al., 2012; Kuznetsov et al., 2011; Layfield et al., 2006). These changes in fluorescence have been attributed to altered NADH/NAD(P)H ratio and the presence of oxidized $FADH_2$, which during mitochondrial ATP production, serve as electron carriers to complex I and II, respectively. The effects of tissue contamination should also be considered although, in our hands, using disaggregated *C. elegans* cells, we have seen minimal autofluorescence in any channel. Nonetheless, one should factor in tissue contamination if studying aged tissues in mammals, which possess higher amounts of lipofuscin, or “age pigment.” The yellow to red autofluorescence of this material (when excited with UV) is thought to consist of highly-oxidized, insoluble proteins and lipids (Pincus et al., 2016).

Finally, it is important to note that some lipids (and probably other metabolites and chemicals) are autofluorescent in the Green or Red channel. We found that palmitoyl-DL-carnitine (AC) suspended alone in MIB is autofluorescent in the Green channel which made ratiometric determination of membrane potential (e.g. JC-9 Red/Green fluorescence) a poor predictor of this quality, especially with depolarized mitochondria (Nguyen et al., 2017). Since AC was not autofluorescent in the Red channel, we were able to normalize the amount of Red JC-9 aggregates (an indicator of membrane potential) to the calculated diameter of mitochondria. This is one solution if your experimental conditions include a chemical that

creates Green autofluorescent aggregates but unfortunately, this becomes more complicated when the added agent is Red fluorescent (e.g. the indicator which demonstrates degree of polarization). In this case, we recommend (1) diluting to prevent aggregates or (2) identifying an alternative Red fluorescence filter set.

### Anticipated Results

Consult Daniele et al., 2016 for additional illustrations and applications of this protocol.

### Time Considerations

Membrane potential is best measured on mitochondria within 1 hour of isolation.

## Acknowledgments

We are very grateful to Erica Moehle and Ryo Higuchi-Sanabria for their helpful and incisive comments during the preparation of this manuscript. This work was funded by a National Institute of Health grant awarded to Andrew Dillin (5R01AG042679-02).

## Literature Cited

Adhihetty PJ, Ljubicic V, Menzies KJ, Hood DA. Differential susceptibility of subsarcolemmal and intermyofibrillar mitochondria to apoptotic stimuli. American Journal of Physiology - Cell Physiology. 2005; 289:C994–C1001. [PubMed: 15901602]

Ahier A, Dai C-Y, Tweedie A, Bezawork-Geleta A, Kirmes I, Zuryn S. Affinity purification of cell-specific mitochondria from whole animals resolves patterns of genetic mosaicism. Nature Cell Biology. 2018:1. [PubMed: 29269947]

Andersson H, Baechi T, Hoechl M, Richter C. Autofluorescence of living cells. Journal of Microscopy. 1998; 191:1–7. [PubMed: 9723186]

Bartolomé, F., Abramov, AY. Mitochondrial Medicine Methods in Molecular BiologyHumana Press; New York, NY: 2015Measurement of Mitochondrial NADH and FAD Autofluorescence in Live Cells; 263-270Available at: https://link.springer.com/protocol/10.1007/978-1-4939-2257-4_23 [Accessed December 12, 2017]

Beavis AD, Brannan RD, Garlid KD. Swelling and contraction of the mitochondrial matrix. I. A structural interpretation of the relationship between light scattering and matrix volume. Journal of Biological Chemistry. 1985; 260:13424–13433. [PubMed: 4055741]

Bondza-Kibangou P, Millot C, Dufer J, Millot JM. Microspectrofluorometry of autofluorescence emission from human leukemic living cells under oxidative stress. Biology of the Cell. 2001; 93:273–280. [PubMed: 11770840]

Brenner S. The Genetics of Caenorhabditis Elegans. Genetics. 1974; 77:71–94. [PubMed: 4366476]

Brys K, Castelein N, Matthijssens F, Vanfleteren JR, Braeckman BP. Disruption of insulin signalling preserves bioenergetic competence of mitochondria in ageing Caenorhabditis elegans. BMC Biology. 2010; 8:91. [PubMed: 20584279]

Byerly L, Cassada RC, Russell RL. The life cycle of the nematode Caenorhabditis elegans: I. Wild-type growth and reproduction. Developmental Biology. 1976; 51:23–33. [PubMed: 988845]

Chen H, Chomyn A, Chan DC. Disruption of Fusion Results in Mitochondrial Heterogeneity and Dysfunction. Journal of Biological Chemistry. 2005; 280:26185–26192. [PubMed: 15899901]

Claude A, Fullam EF. AN ELECTRON MICROSCOPE STUDY OF ISOLATED MITOCHONDRIA. The Journal of Experimental Medicine. 1945; 81:51–62. [PubMed: 19871443]

Cossarizza A, Baccaranicontri M, Kalashnikova G, Franceschi C. A New Method for the Cytofluorometric Analysis of Mitochondrial Membrane Potential Using the J-Aggregate Forming Lipophilic Cation 5,5′,6,6′-Tetrachloro-1,1′,3,3′-tetraethylbenzimidazolcarbocyanine Iodide (JC-1). Biochemical and Biophysical Research Communications. 1993; 197:40–45. [PubMed: 8250945]

Cossarizza A, Ceccarelli D, Masini A. Functional Heterogeneity of an Isolated Mitochondrial Population Revealed by Cytofluorometric Analysis at the Single Organelle Level. Experimental Cell Research. 1996; 222:84–94. [PubMed: 8549677]

Cossarizza, A., Salvioli, S. Current Protocols in CytometryJohn Wiley & Sons, Inc; 2001Flow Cytometric Analysis of Mitochondrial Membrane Potential Using JC-1. Available at: http://onlinelibrary.wiley.com/doi/10.1002/0471142956.cy0914s13/abstract [Accessed October 11, 2015]

Cottet-Rousselle C, Ronot X, Leverve X, Mayol JF. Cytometric assessment of mitochondria using fluorescent probes. Cytometry Part A. 2011; 79A:405–425.

Cox GN, Kusch M, Edgar RS. Cuticle of Caenorhabditis elegans: its isolation and partial characterization. The Journal of Cell Biology. 1981; 90:7–17. [PubMed: 7251677]

Daniele JR, Heydari K, Arriaga EA, Dillin A. Identification and Characterization of Mitochondrial Subtypes in Caenorhabditis elegans via Analysis of Individual Mitochondria by Flow Cytometry. Analytical Chemistry. 2016; 88:6309–6316. [PubMed: 27210103]

Degli Esposti, M. Chapter 4 Assessing functional integrity of mitochondria in vitro and in vivo. In: B-M, Biology, C., editorsMitochondriaAcademic Press; 200175-96Available at: http://www.sciencedirect.com/science/article/pii/S0091679X01650052 [Accessed May 11, 2016]

Gandre S, van der Bliek AM. Mitochondrial division in Caenorhabditis elegans. Methods in Molecular Biology (Clifton, NJ). 2007; 372:485–501.

Gómez-Puyou A, Sandoval F, Chávez E, Tuena M. On the role of K+ on oxidative phosphorylation. The Journal of Biological Chemistry. 1970; 245:5239–5247. [PubMed: 4319236]

Gravance C, Garner D, Baumber J, Ball B. Assessment of equine sperm mitochondrial function using JC-1. Theriogenology. 2000; 53:1691–1703. [PubMed: 10968415]

Head BP, Zulaika M, Ryazantsev S, van der Bliek AM. A novel mitochondrial outer membrane protein, MOMA-1, that affects cristae morphology in Caenorhabditis elegans. Molecular Biology of the Cell. 2011; 22:831–841. [PubMed: 21248201]

Hicks KA, Howe DK, Leung A, Denver DR, Estes S. In Vivo Quantification Reveals Extensive Natural Variation in Mitochondrial Form and Function in Caenorhabditis briggsae. PLoS ONE. 2012; 7:e43837. [PubMed: 22952781]

Jagasia R, Grote P, Westermann B, Conradt B. DRP-1-mediated mitochondrial fragmentation during EGL-1-induced cell death in C. elegans. Nature. 2005; 433:754–760. [PubMed: 15716954]

Knight VA, Wiggins PM, Harvey JD, O'Brien JA. The relationship between the size of mitochondria and the intensity of light that they scatter in different energetic states. Biochimica Et Biophysica Acta. 1981; 637:146–151. [PubMed: 7284354]

Kuang J, Ebert PR. The failure to extend lifespan via disruption of complex II is linked to preservation of dynamic control of energy metabolism. Mitochondrion. 2012; 12:280–287. [PubMed: 22122855]

Kuznetsov AV, Margreiter R, Amberger A, Saks V, Grimm M. Changes in mitochondrial redox state, membrane potential and calcium precede mitochondrial dysfunction in doxorubicin-induced cell death. Biochimica et Biophysica Acta (BBA) - Molecular Cell Research. 2011; 1813:1144–1152. [PubMed: 21406203]

Layfield R, Cavey JR, Najat D, Long J, Sheppard PW, Ralston SH, Searle MS. p62 mutations, ubiquitin recognition and Paget's disease of bone. Biochemical Society Transactions. 2006; 34:735–737. [PubMed: 17052185]

Lemire BD, Behrendt M, DeCorby A, Gášková D. C. elegans longevity pathways converge to decrease mitochondrial membrane potential. Mechanisms of Ageing and Development. 2009; 130:461–465. [PubMed: 19442682]

Monici, M. Biotechnology Annual ReviewElsevier; 2005Cell and tissue autofluorescence research and diagnostic applications; 227-256Available at: http://www.sciencedirect.com/science/article/pii/S1387265605110072 [Accessed December 12, 2017]

Narendra D, Tanaka A, Suen DF, Youle RJ. Parkin is recruited selectively to impaired mitochondria and promotes their autophagy. The Journal of Cell Biology. 2008; 183:795–803. [PubMed: 19029340]

Nguyen TB, Louie SM, Daniele JR, Tran Q, Dillin A, Zoncu R, Nomura DK, Olzmann JA. DGAT1-Dependent Lipid Droplet Biogenesis Protects Mitochondrial Function during Starvation-Induced Autophagy. Developmental Cell. 2017; 42:9–21e5. [PubMed: 28697336]

Ogata E, Rasmussen H. Valinomycin and Mitochondrial Ion Transport*. Biochemistry. 1966; 5:57–66. [PubMed: 5940319]

O'Toole JF, Patel HV, Naples CJ, Fujioka H, Hoppel CL. Decreased cytochrome c mediates an age-related decline of oxidative phosphorylation in rat kidney mitochondria. Biochemical Journal. 2010; 427:105–112. [PubMed: 20100174]

Parone PA, Da Cruz S, Tondera D, Mattenberger Y, James DI, Maechler P, Barja F, Martinou JC. Preventing Mitochondrial Fission Impairs Mitochondrial Function and Leads to Loss of Mitochondrial DNA. PLoS ONE. 2008; 3:e3257. [PubMed: 18806874]

Petit PX. Flow Cytometric Analysis of Rhodamine 123 Fluorescence during Modulation of the Membrane Potential in Plant Mitochondria. Plant Physiology. 1992; 98:279–286. [PubMed: 16668625]

Pincus Z, Mazer TC, Slack FJ. Autofluorescence as a measure of senescence in C. elegans: look to red, not blue or green. Aging. 2016; 8:889–898. [PubMed: 27070172]

Reers M, Smith TW, Chen LB. J-aggregate formation of a carbocyanine as a quantitative fluorescent indicator of membrane potential. Biochemistry. 1991; 30:4480–4486. [PubMed: 2021638]

Saunders JE, Beeson CC, Schnellmann RG. Characterization of functionally distinct mitochondrial subpopulations. Journal of Bioenergetics and Biomembranes. 2013; 45:87–99. [PubMed: 23080405]

Schaue D, Ratikan JA, Iwamoto KS. Cellular Autofluorescence following Ionizing Radiation. PLOS ONE. 2012; 7:e32062. [PubMed: 22384140]

Sharpley MS, Marciniak C, Eckel-Mahan K, McManus M, Crimi M, Waymire K, Lin CS, Masubuchi S, Friend N, Koike M, et al. Heteroplasmy of Mouse mtDNA Is Genetically Unstable and Results in Altered Behavior and Cognition. Cell. 2012; 151:333–343. [PubMed: 23063123]

Shimada T, Morizono T, Yoshimura T, Murakami M, Ogura R. Scanning Electron Microscopy of Isolated Mitochondria. Journal of Electron Microscopy. 1978; 27:207–208. [PubMed: 103989]

Smiley ST, Reers M, Mottola-Hartshorn C, Lin M, Chen A, Smith TW, Steele GD, Chen LB. Intracellular heterogeneity in mitochondrial membrane potentials revealed by a J-aggregate-forming lipophilic cation JC-1. Proceedings of the National Academy of Sciences. 1991; 88:3671–3675.

Tsang WY, Lemire BD. Stable heteroplasmy but differential inheritance of a large mitochondrial DNA deletion in nematodes. Biochemistry and Cell Biology = Biochimie Et Biologie Cellulaire. 2002; 80:645–654. [PubMed: 12440704]

Vander Heiden MG, Chandel NS, Williamson EK, Schumacker PT, Thompson CB. Bcl-xL Regulates the Membrane Potential and Volume Homeostasis of Mitochondria. Cell. 1997; 91:627–637. [PubMed: 9393856]

Wolken GG, Arriaga EA. Simultaneous measurement of individual mitochondrial membrane potential and electrophoretic mobility by capillary electrophoresis. Analytical Chemistry. 2014; 86:4217–4226. [PubMed: 24673334]

Yamada A, Yamamoto T, Yamazaki N, Yamashita K, Kataoka M, Nagata T, Terada H, Shinohara Y. Differential Permeabilization Effects of Ca2+ and Valinomycin on the Inner and Outer Mitochondrial Membranes as Revealed by Proteomics Analysis of Proteins Released from Mitochondria. Molecular & Cellular Proteomics. 2009; 8:1265–1277. [PubMed: 19218587]

Yang W, Hekimi S. A Mitochondrial Superoxide Signal Triggers Increased Longevity in Caenorhabditis elegans. PLoS Biol. 2010; 8:e1000556. [PubMed: 21151885]

Ylikallio E, Suomalainen A. Mechanisms of mitochondrial diseases. Annals of Medicine. 2011; 44:41–59. [PubMed: 21806499]

## Significance Statement

The health of mitochondria is of utmost importance to cell function and to the organism as a whole. To preserve the fitness and function of this organelle, cellular mitochondrial quality control mechanisms exist and directly impact membrane potential, size, and substructure. Populations of mitochondria differ dramatically within individual cells, and even more across different cell types, tissues, and throughout aging. Here we present a robust and high-throughput technique to detect and quantitatively measure such phenotypic heterogeneity at the organelle level to gain insight into mitochondrial biology as it impacts development, aging, and genetic disease.

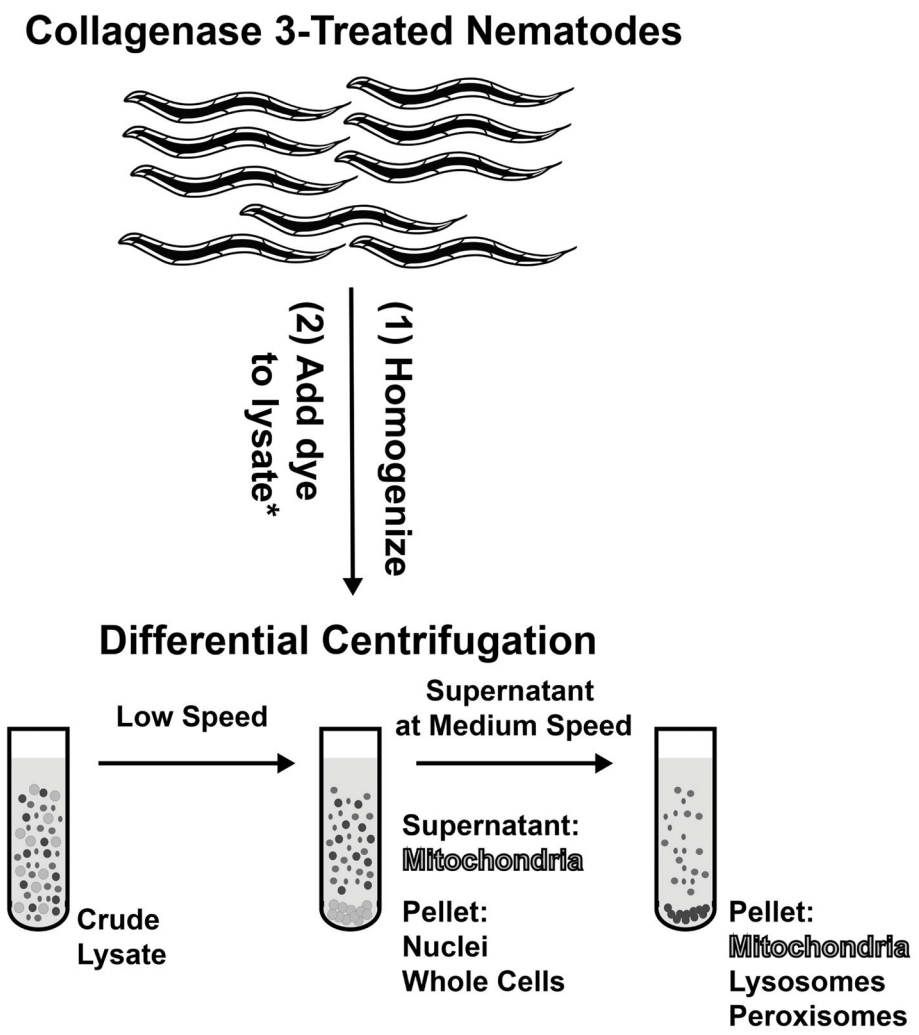


**Figure 1. Illustration of crude mitochondrial isolation procedure**

*See note in *Part I, Step 5* to know the controls where dye is not added.

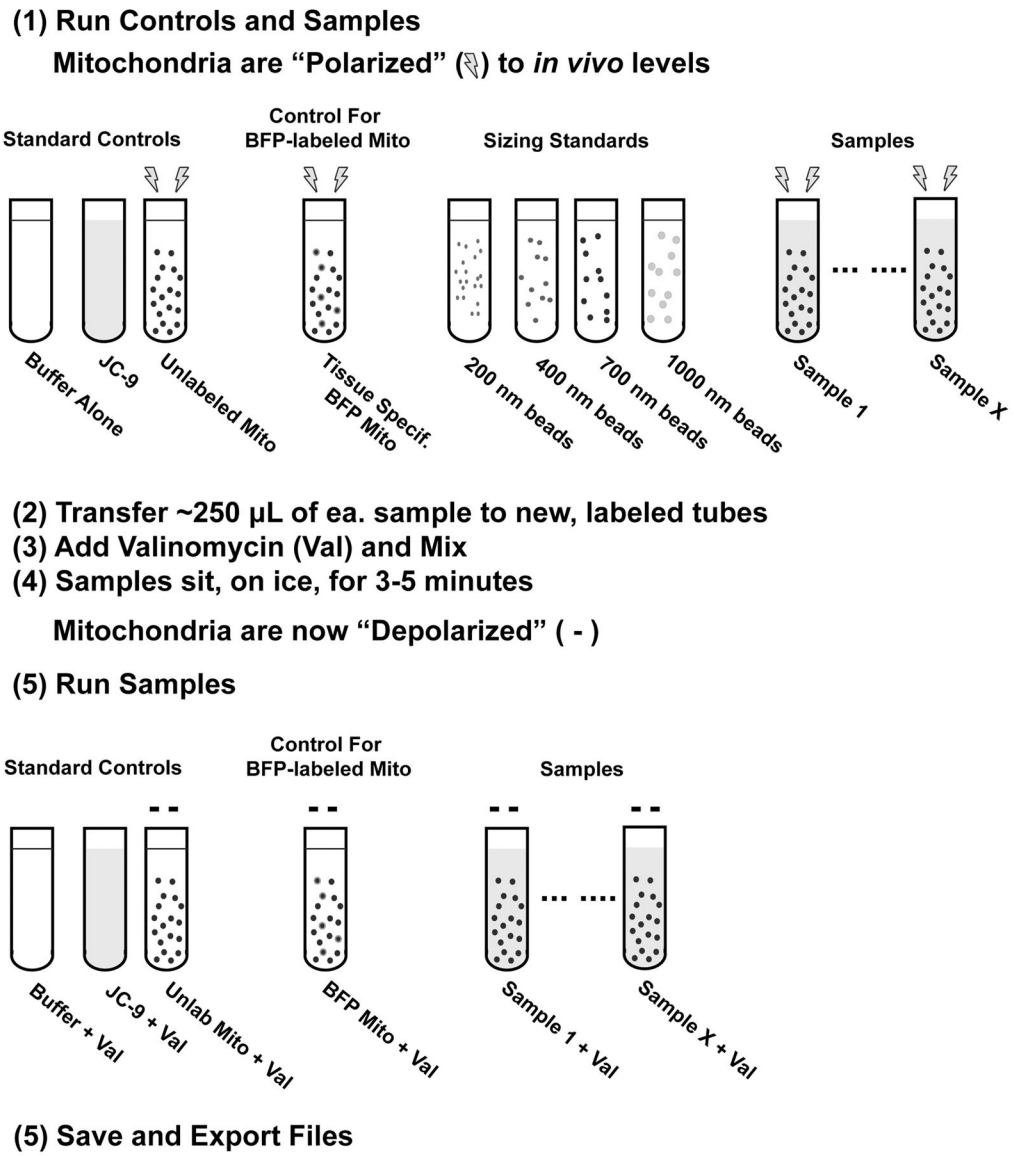


**Figure 2.**
Flow chart for running samples and controls in a standard experiment.

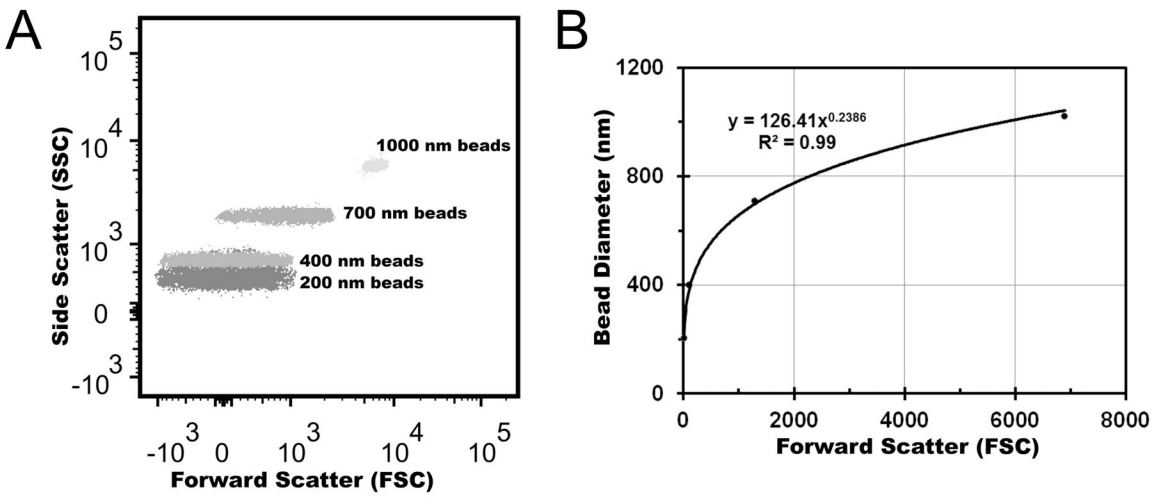


**Figure 3. Extrapolation of mitochondrial diameter from the forward scatter of polymer microspheres of known size**

**(A)** Forward and side scatter for a range of bead sizes. There is some overlap between the 200 nm and 400 nm beads signal. Although this does not change the medians this overlap could be better appreciated using a contour plot. **(B)** Median FSC was chosen for each bead diameter and plotted against the actual diameter. A best-fit curve was calculated and this equation was used to perform the conversion.

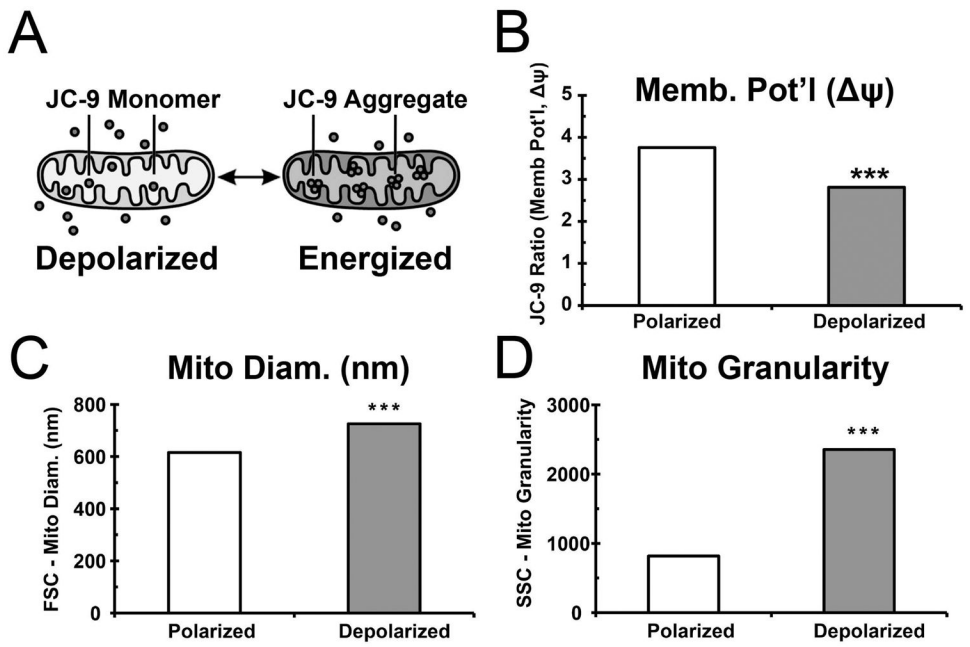


**Figure 4. JC-9 can label both polarized and depolarized isolated mitochondria**

**(A)** JC-9 is a mitochondrial dye that exists in a monomeric (green fluorescent, **light grey, left**) state but forms red fluorescent aggregates (**dark grey, right**) when mitochondria are polarized. Red fluorescence increases relative to an increase in mitochondrial membrane potential (Δψ). **(B)** Representative use of the **Red/Green "JC-9 fluorescence ratio"** in a comparison of polarized and depolarized mitochondria. Median Red/Green "JC-9 fluorescence ratio" is higher for polarized mitochondria due to formation of more aggregate (red). **(C)** Mitochondrial diameter (nm), derived from Forward scatter (FSC), increases when mitochondria are depolarized (with valinomycin, **gray bars**) while **(D)** side scatter (SSC), mitochondria granularity/substructure, greatly increases upon depolarization. All values shown are medians. '***' = $P<0.0001$ by Mann-Whitney test. Adapted with permission from Daniele et al., 2016.

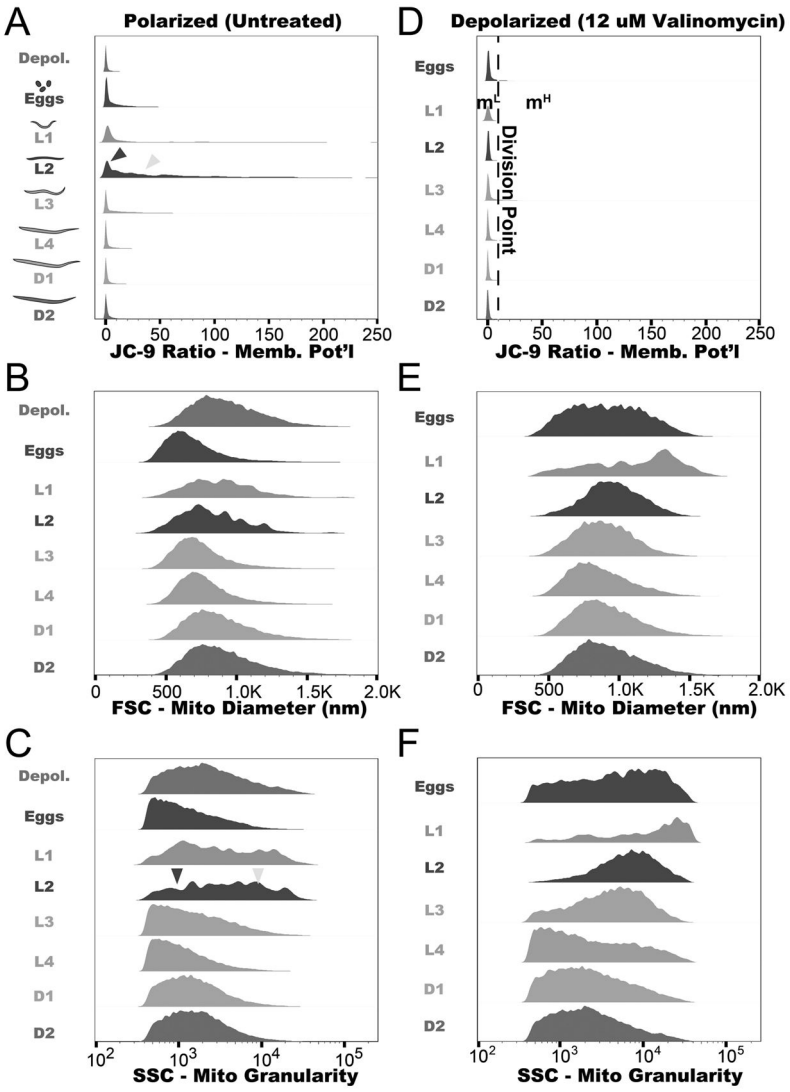


**Figure 5. Effects of depolarization on membrane potential, mitochondrial diameter, and mitochondrial granularity**

**(A–F)** Distribution of $\Delta\psi$ **(A,D)**, mito size **(B,E)**, and mito granularity/substructure **(C,F)**. The presence of mitochondria with high $\Delta\psi$ **(A)**, highly granular **(C)**, (called "$m^H$", **light arrowheads**) appears to account for the dramatic rise in median JC-9 ratio between L1-L3 stages of nematode development. On the other hand, mitochondria with low $\Delta\psi$ **(A)** and low texture **(C)** are present through all stages ("$m^L$", **dark arrowheads**) and these represent the majority subtype in the Egg and L4-D2 stages of development. The distribution of mitochondrial properties for the "depolarized" or "ground state" is shown in **D–F**. "Depol." = "depolarized". Adapted with permission from Daniele et al., 2016.